ACES Asian Chemical Editorial Society

DOI: 10.1002/cnma.202000521

CHEMNANOMAT
Full Paper

3D Silver Dendrites for Single-molecule Imaging by Surface-enhanced Raman Spectroscopy

Hanna V. Bandarenka,*[a, b] Nadzeya V. Khinevich,[b, e] Aliaksandr A. Burko,[b] Sergey V. Redko,[b] Siarhei A. Zavatski,[b, c] Uladzislau A. Shapel,[d, e] Kahramon Z. Mamatkulov,[f] Maria Yu. Vorobyeva,[f] and Grigory M. Arzumanyan*[f]

Abstract: Discovery of surface-enhanced Raman scattering (SERS) followed by evolution of optical systems and nano-engineering approaches has paved a path to detection of essential organic molecules on solid SERS-active substrates from solutions at concentrations attributed to single-molecule ones, i.e. below 10^{-15} M. However, in practical terms confident SERS-imaging of single molecules is still quite a challenge. In present work, we fabricated and comprehensively characterized tightly-packed 3D silver dendrites with prevalent chevron morphology that demonstrated ultrahigh sensitivity as SERS-active substrates resulted in 10^{-18} M detection limit. Using these substrates we achieved SERS-imaging of single 5-thio-2-nitrobenzoic acid (TNB) molecule released from the attomolar-concentrated solution of of 5,5′-dithio-bis-[2-nitrobenzoic acid] (DTNB), which is vital compound for chemical and biomedical analysis. In contrast to generally accepted belief about adsorption of only uniform monomolecular TNB layer on surface of silver nanostructures, we showed formation of a coating constituted by TNB layer and DTNB nanoclusters on the dendrites' surface at 10^{-6}–10^{-12} M DTNB concentrations confirmed by presence/absence of disulfide bonds signature in the SERS-spectra and by scanning electron microscopy. DTNB concentrations below 10^{-14} M resulted in adsorption of TNB molecules in separated spots on the surface of silver nanostructures.

1. Introduction

In recent decades, sensing technologies have become so powerful that today diverse sensors pervade our daily lives giving a raise to tightening our requirements to their accuracy, precision, and analysis speed, which are especially critical for the molecular detection in medicine and pharmaceutics, forensics and security, environmental monitoring and other areas of human life. To move towards new frontiers in molecular sensing, optical spectroscopies and nanotechnology have been combined.[1–3] SERS-spectroscopy is a successful example of such a combination that not only reveal the presence or absence of a target molecule in an analyzing media,[4,5] but also recognize its fingerprint and shows sensitivity down to the single molecule level.[6]

An abnormal increase of a Raman signal from analyte molecules is observed when they are adsorbed on or located in a close vicinity to SERS-active substrates.[7] These substrates are important tools of the SERS-spectroscopy and comprise nanoparticles (NPs) of noble metals in colloids[8,9] or immobilized on soft materials including paper,[10–12] fabrics,[13,14] polymers,[15,16] plant derivatives[17,18] and the hard ones made of dielectrics[19–21] and semiconductors.[22–24] Each substrate's type has its own purpose and advantages. NPs from the colloids can be introduced into cells to analyze their molecular composition.[25] Namely liquid substrates are known as leaders in detection limits.[26,27] On the other hand, the metallic NPs in solutions may result in some irreproducibility of the SERS intensity in a series of measurements due to aggregation. Some attempts have been made to overcome this problem.[28] Considering a practical use, liquid SERS-active substrates are not always convenient for routine SERS-measurements. In contrast, solid SERS-active materials demonstrate better stability and repeatability of their properties due to orderliness and stable position of metallic NPs on the substrate. Additionally, they are more user-friendly and can be implemented in a wide practice since do not require a specific training for the staff to operate with them.

It is generally accepted that an enhancement of the Raman signal from molecules in a course of the SERS-measurements emerges due to chemical and electromagnetic mechanisms.[29,30] The first one is caused by a charge transfer between the SERS-active substrate and an analyte molecule and is accompanied by an increase of the Raman intensity up to three orders of magnitude. The second mechanism involves collective oscilla-

[a] *Prof. H. V. Bandarenka*
The Polytechnic School, Ira A. Fulton Schools of Engineering, Arizona State University, Mesa 85212, AZ (USA)
E-mail: hbandare@asu.edu
[b] *Prof. H. V. Bandarenka, N. V. Khinevich, A. A. Burko, S. V. Redko, S. A. Zavatski*
Micro- and Nanoelectronics Department, Belarusian State University of Informatics and Radioelectronics, Minsk 220013 (Belarus)
E-mail: h.bandarenka@bsuir.by
[c] *S. A. Zavatski*
Nanophotonics and Metrology Laboratory, Swiss Federal Institute of Technology Lausanne (EPFL), Lausanne 1015 (Switzerland)
[d] *U. A. Shapel*
Lyceum of Belarusian State University, Minsk 220030 (Belarus)
[e] *N. V. Khinevich, U. A. Shapel*
Kaunas University of Technology, Kaunas 44249 (Lithuania)
[f] *Dr. K. Z. Mamatkulov, M. Y. Vorobyeva, Prof. G. M. Arzumanyan*
Laboratory of Neutron Physics, Joint Institute for Nuclear Research, Dubna 141980 (Russia)
E-mail: arzuman@jinr.ru

© 2020 Wiley-VCH GmbH

tions of free electrons (plasmons) in the metallic nanostructures upon a laser excitation. If frequencies of these oscillations and excitation light coincide, SPR is observed, which is associated with a giant jump in a strength of an electromagnetic field near the surface of the metallic nanostructures. As the result, the Raman signal from the adsorbed molecule is enhanced up to several orders of magnitude.[31] SPR modes depend on a metallic NPs composition, dimensions and a dielectric constant of the surrounding medium.[32] A key parameter for tuning the SPR spectral position is the geometry (shape, dimensions and spatial location) of the metallic NPs. Silver (Ag) and gold (Au) nanostructures in the form of 2D NPs or 3D fractal dendrites are the most popular SERS-active substrates.[33–36] 3D dendritic substrates demonstrate two advantages in the SERS spectroscopy compared to 2D nanostructures. First, the SPR spectral band in fractal elements is wider than that in 2D nanostructures. This is due to transverse and longitudinal electromagnetic modes in the dendrites that have variable dimensions. Their oscillation frequencies depend on the diameter and length of trunks and lateral branches of the dendrites. This feature of the dendritic structures provides an excitation and the SERS-activity upon a wide range of laser wavelengths. Second, 3D dendritic substrates exhibit an extremely developed morphology that possesses much more hot spots compared to the 2D NPs. The hot spots appear between closely located metallic nanostructures and present small areas of overlapped electromagnetic fields. As a result, a very strong SERS signal enhancement occurs in these points. A great number of the hot spots is extremely important for a practical implementation of the SERS-active substrates because this will provide the SERS-activity even in case of relatively low laser power including portable instrumentation. Based on the above mentioned, the dendritic SERS-active substrates have been considered promising to provide new records in the detection limit and effectiveness over an expanded range of excitation wavelengths. For some years major attention had been directed to colloidal dendritic particles fabricated by reduction of silver or gold ions in solutions, but the single molecule detection limit had not been achieved for them.[37–39]

It should be noted that the SERS detection of molecules at concentrations lower than 10^{-15} M was mostly realized for R6G, which has large Raman scattering cross-section, and was usually accompanied by a long lasting flow monitoring of R6G mixture with colloids of metallic NPs[26] or concentrating the R6G molecules in a small area of solid SERS-active substrates[40]. Such approaches do not result in a reliable revealing of distribution of single molecules over the nanostructured metallic surface, *i.e.* to achieve a single-molecule SERS-imaging. Since the beginning of the 2000's, the SERS imaging of R6G, DTNB, adenine and other molecules at concentrations close to the single-molecule level have been demonstrated with a variety of the SERS-active substrates including but not limited to silver colloid aggregates[41,42] and nanoshells.[43] However, a quantitative assessment of imaged molecules has usually been based on generally approved assumptions on formation of single molecular layer over the metallic nanostructures and any specific adsorption behavior has not been considered.

In present work, we pursued a goal to achieve a reliable single-molecule imaging through utilizing solid SERS-active substrates based on volumetric silver dendrites enriched with a great number of hot spots. A growth of the 3D densely-packed layer of the silver dendrites was facilitated by using a template of macroporous silicon (macro-PS), which has already been reported as a suitable basis for the SERS-active substrates.[44] DTNB was selected as an analyte for the detection since it is an important reagent in chemical and biomedical analysis including but not limited to bacteria detection[45] and quantification of protease activity.[46] The unique feature of the DTNB molecule is its breaking up to two TNB^{2-} ions in presence of atoms of transition metals. These ions are known to be adsorbed on the metallic surface as a monomolecular TNB layer. Therefore, an informative SERS-spectrum (containing three main characteristic bands at approximately 1076, 1335, and 1556 cm^{-1}) obtained from the area overlapped with a submicron diameter laser spot carries a signature of the TNB products at the amount attributed to the single molecule concentration.

2. Results and Discussion

2.1. Morphology of the silver dendrites on macroporous silicon

Figure 1 shows SEM and atomic force microscopy (AFM) images of the macro-PS sample that was processed in the solution of $AgNO_3$ salt for 3 minutes. A developed network of the Ag NPs and Ag dendrites was formed on the surface of the macro-PS. It was hard to correctly evaluate a density of the Ag NPs formed at the surface of the Si skeleton since they were covered by dendrites. A thickness of the dendritic layer was rather uniform (3–3.5 μm). As it can be seen from the sample cross-section (Figure 1A), an external surface of the macro-PS was rough and the Ag NPs and Ag dendrites were formed on it. The dendrites were directed both vertically and laterally along the surface of the macro-PS. A length of central trunks of the lateral dendrites reached 20–25 μm, and the lateral branches – about 3–7 μm. There was a large number of additional sprouts of 100–300 nm length on the lateral branches of the dendrites.

The structure of the dendrites was extremely rich and all their elements (central trunks and lateral branches) consisted of well-distinguishable Ag NPs. Moreover, it is clearly observed, that Ag dendrites were formed on the sharp parts of the rough surface of the Si skeleton. Advantageously, the dendrites were formed at the periphery of the pore entrances and their number for a single pore is about 9–12 pieces.

Some of the dendrites were located almost vertically and they had a short length of 1.0–2.5 μm. The number of the lateral dendrites was smaller, but they were much longer than the vertical dendrites. The lateral dendrites were flattened and a majority of them resemble fern leaves with a chevron structure (Figure 1A). The main and secondary branches of the chevron-like dendrites had the mean diameter of 80 and 40 nm respectively. A negligible number of the dendrites had disordered structure and much larger branches' diameters (Fig-

© 2020 Wiley-VCH GmbH
These are not the final page numbers!

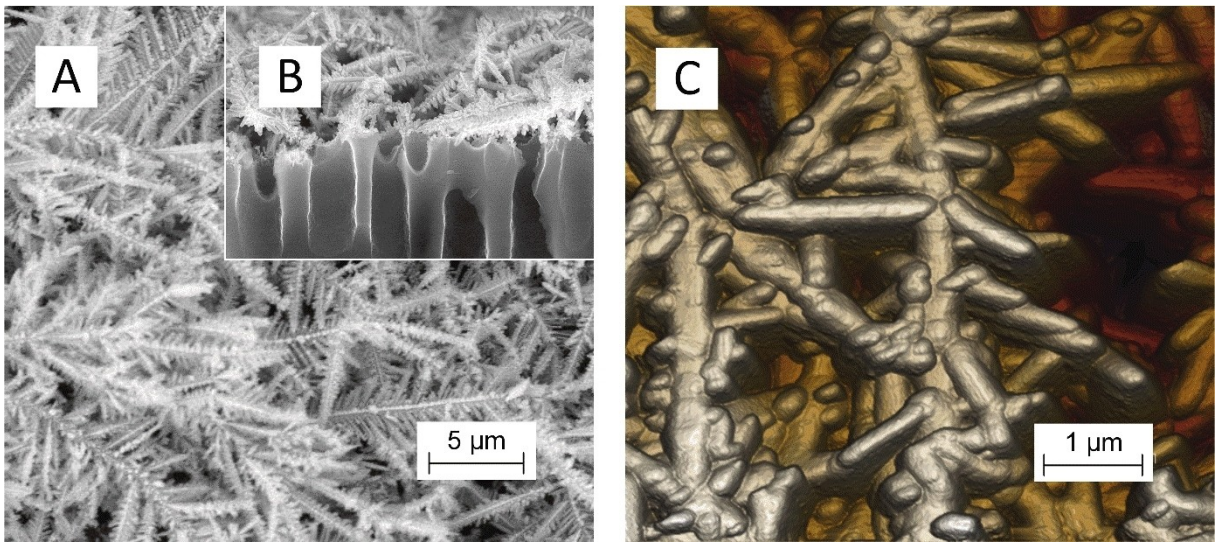

Figure 1. SEM (A) top, (B) cross section and AFM (C) top images of the silver dendrites on macro-PS.

ure 1B). It should be noted that no dendrites were detected within the pore channels. The average size of the Ag NPs composing the dendrites was about 50 nm. A number of the Ag NPs per unit of the analyzed area reached $5.5 \cdot 10^{10}$ cm^{-2}, which is almost one order of magnitude more than for the samples formed on the ion-track templates provided the recently reported 10^{-15} M DTNB detection limit.[47] Analysis of the SEM images presented in Figure 1 also showed that a coverage of the macro-PS surface with the Ag NPs constituting the dendrites reached 90–95%. The data presented in Figure 1, clearly indicated a predominant Ag deposition on the external surface of macro-PS and non-precipitation of Ag on the pores' walls. This result is fundamentally important and interesting. We believe that the selective Ag deposition was realized due to a combination of ion etching the thin surface layer of the Si skeleton followed by the Ag deposition from the solution containing $AgNO_3$ salt and a small amount of hydrofluoric acid. The metallic nanostructures are usually formed inside the pores of the PS template. The Si skeleton is known to be enriched with surface states (broken bonds on cracks and protrusions, *etc.*). They are favorable places for a nucleation of the metallic NPs, which thus grow in bottoms and walls of the pores as well as on tops of the Si skeleton. After nucleation, the NPs are increased in sizes until the moment of the PS surface is completely covered with them. As a result, there is a less number of electrons from the Si skeleton to supply metallic ions from the solution for reduction to the atomic form. This limitation initiates localizing the silver crystallization in rare points of the substrate. These silver nanocrystals grow upon the lack of electrons from the Si skeleton and excess of the Ag ions from the solution. In our case at the very first moment of the contact between the macro-PS and the Ag salt solution, the Ag nucleation dominated on the outer surface of the Si skeleton as it was previously roughened by plasma etching. These primarily formed Ag NPs played a pronounced catalytic role and then silver was deposited only on the Si skeleton tops and did not settle inside the pores' channels. Therefore, an internal surface of the pores was open to constantly supply the silver atoms with electrons. As a result, at the moment of the saturation of the external surface of macro-PS with the Ag NPs, more centers of the dendrites' growth appeared and the final silver layer was denser comparing to that on the conventionally used porous templates or mono-Si. It should also be noted that at an absence of HF in the solution, the Ag deposition is promptly stopped as the Si surface is oxidized while the silver reduction. In this work, we added HF to remove the silicon oxide promoting further electrons availability. We also observed an effect that is important for the practical application of the SERS-active substrates: the layer of the Ag dendrites on the macro-PS had a stronger adhesion to the substrate in contrast to those on other substrates reported elsewhere.[48] This may provide for users to safely keep the silvered macro-PS in the analyte solutions for a long time avoiding separation of the dendritic layer.

2.2. Optical properties of the silver dendrites on macroporous silicon

The reflectance spectrum of the Ag layers deposited on the macro-PS is shown in Figure 2A. The reflectance minima associated with the light absorption due to SPR modes was observed: centered around 473, 633 and 785 nm. The band at 473 nm corresponded to the transverse dipole SPR mode of the Ag NPs while two bands in the range of longer wavelengths appeared due to the longitudinal dipole and quadruple SPR modes of elongated elements of Ag dendrites.[49]

The better understanding of the morphology effect on the SERS measurements can be given by a computer simulation of an electric field in the silver structures on the macro-PS.

© 2020 Wiley-VCH GmbH

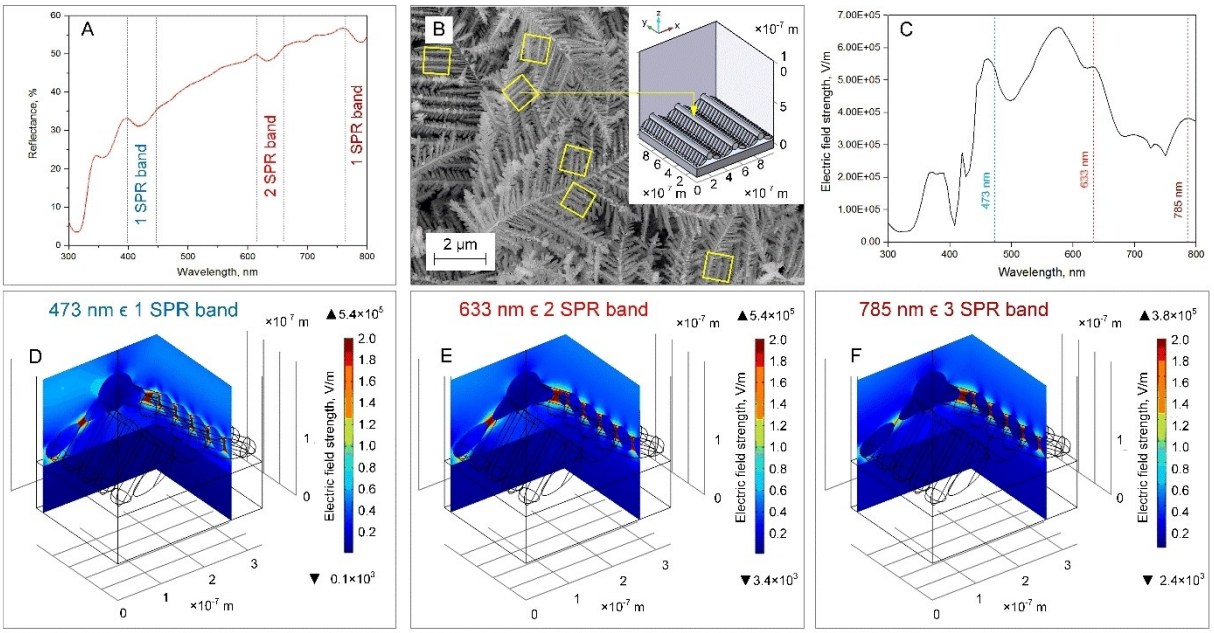

Figure 2. Reflectance spectrum (A) of the silver dendrites on macro-PS; area (B) selected for the simulation of the electric field strength in the silver dendrites on macro-PS; (C) electric field strength simulated in the point between dendrite branches vs. excitation wavelength; distribution of the electric field strength (D–F) induced by light with wavelengths corresponding to the SPR bands.

Figure 2B presents examples of the square area selected for the simulation of the electric field in dendrites. Figure 2C–F additionally to the reflectance spectrum shows the results of simulations performed for the fabricated and experimentally studied Ag dendrites. Following the information on the composition of PS[50] we selected a refractive index of the underlying substrate corresponding to that of an amorphous silicon. The silver dendrites on the macro-PS were modeled with dense chevron-like elements that had an 80 nm and 40 nm diameter for the main and secondary branches, respectively. Such chevron-like structures were selected for the simulation since they dominated in the dendritic film as described in the 2.1 subsection.

Simulation of the electric field in a point between two branches of the silver chevron showed it had the highest strength around 460, 570, 630 and 785 nm of excitation wavelength (Figure 2C).

We assume that the real silver dendritic structure was characterized by domination of branches with an aspect ratio, which is more favorable for longitudinal modes resulting in red and near infrared SPR bands but not in green one observed while simulation of electric field for the modelled chevron structure. However, we showed that the silver dendrite structures had evenly distributed areas with an electric field enhancement upon excitation with light of 473, 633 and 785 nm wavelengths (Figure 2D–F). Positions of the hot spots in the chevron-like structures are similar for these three wavelengths because the same plasmon resonance modes contribute to the electric field enhancement. On the other hand, maximal electric strength values are different strongly depending on the wavelength of the excitation light as seen from the numbers over the color bars (Figure 2D–F). This helps to identify an excitation wavelength, which better meets resonant conditions for the SERS-spectroscopy with the silver dendrites.

2.3. SERS-measurements

DTNB molecules are known to be broken in TNB residues that are adsorbed on the silver nanostructures via –S bond. Thus we expected to observe a signature of TNB while the SERS-spectroscopy. The SERS-measurements were performed by mapping three areas (24×24 μm^2) on the SERS-active substrate. We recorded three maps on each sample for the 10^{-6}–10^{-16} M concentrations. In case of 10^{-18} M DTNB solution, we scanned 24×24 μm^2 areas in series until the point with analyte signature was found. As a rule, each 6th or 7th map contained informative signal. This was repeated for three SERS-active substrates to prove reliability of the analyte detection. Figure 3 shows the average SERS-spectra of the analyte molecules adsorbed on the Ag dendrites from solutions at 10^{-6}–10^{-18} M concentrations.

Each spectrum contained the bands typical for the analyte including 1076, 1155, 1335 and 1556 cm^{-1} that were prominent even at attomolar concentration.[51] The 510 cm^{-1} band, which is S–S band fingerprint,[52] was observed in the SERS-spectra collected from the silver dendrites kept in the 10^{-6}–10^{-12} M solutions. This signified about presence of large amount of DTNB molecules in the adsorbed layer of analyte. We expected to see just TNB spectra because of breaking the disulfide bonds of the DTNB molecules, which would have led to single TNB layer adsorption on the dendrites' surface. However, such SERS-

© 2020 Wiley-VCH GmbH

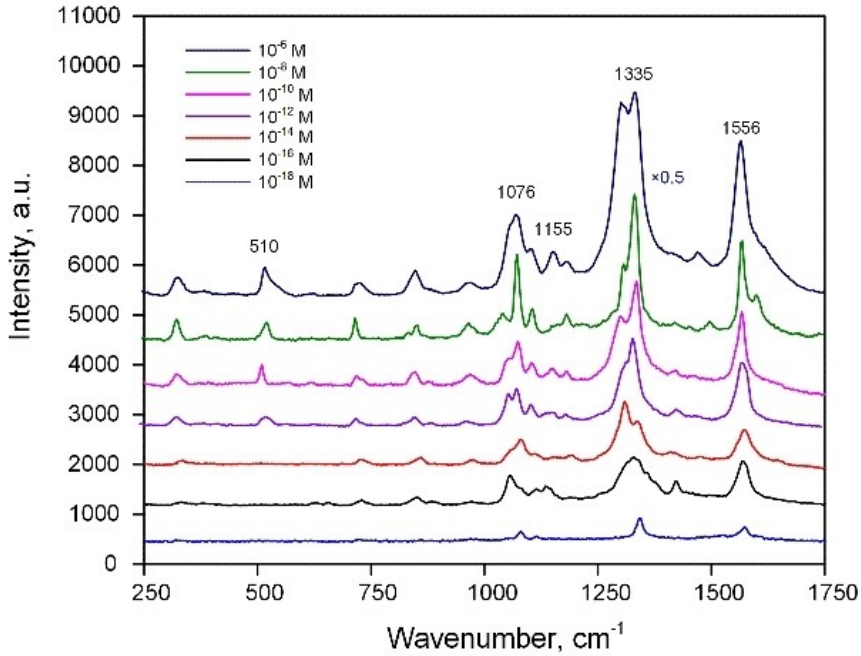

Figure 3. Average SERS spectra for three maps of the Ag dendrites/macro-PS kept in the DTNB solutions with different concentrations. The SERS-spectra were collected under identical conditions (×40 objective, $(1 \pm 0.2) \cdot 10^5$ W/cm^{-2} laser power density, 1 s exposure for each point). The intensity axis is the same for each SERS-spectrum.

spectra were typical only for the samples subjected to immersion in the 10^{-14}–10^{-18} M solutions.

Pursuing a goal to find out reasons for this effect, we studied the SEM images of the samples at the high magnification. Figure 4 presents SEM top views of the SERS-active substrate before and after adsorption of analyte molecules from solutions at 10^{-6}–10^{-12} M concentrations.

Surprisingly, nanoclusters of unknown nature were observed on the Ag dendrites after keeping in the DTNB solutions. It should be noted that we analyzed the SEM images of the samples at all DTNB concentrations. Nanoclusters were visually identified only on the SEM images of the samples with the concentrations of 10^{-6}–10^{-12} M. The number of the nanoclusters was found to decrease at the concentration lowering, but their dimensions were almost constant for all the samples. The nanoclusters had a shape of a hemisphere with a mean diameter of ~7 nm and a volume of about 90 nm^3. These clusters were not observed on the fresh SERS-active substrate (Figure 4A) and therefore we believe they can be composed of only analyte molecules. It is generally accepted that molecules containing disulfide bonds are adsorbed on the gold and silver surfaces via S atom and self-organized in a monomolecular layer through van der Waals forces between alkyl groups[53]. In our case, the DTNB chemical compound was the molecule with S–S bond and TNB was its product adsorbed on the silver atom, which volumetric representations are shown in Figure 5. Volumes occupied by the DTNB and TNB molecules were calculated as 0.34 nm^3 and 0.17 nm^3, respectively.

However, presence of the nanoclusters called into a question the belief in monomolecular TNB adsorption. We suppose that the nanoclusters were formed while drying an adsorbed layer of the analyte molecules to reduce its surface

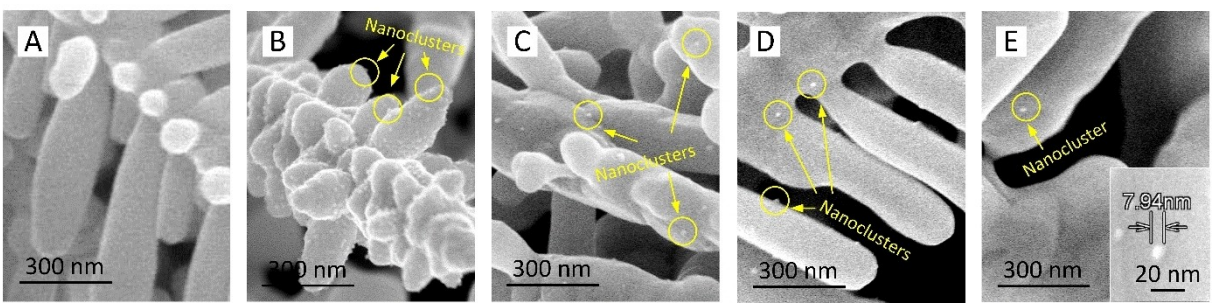

Figure 4. SEM top views of the Ag dendrites (A) before and (B–E) after immersion in DTNB solutions of the (B) 10^{-6} M, (C) 10^{-8} M, (D) 10^{-10} M and (E) 10^{-12} M concentrations. Inset shows SEM top view of a single nanocluster at a higher magnification.

© 2020 Wiley-VCH GmbH

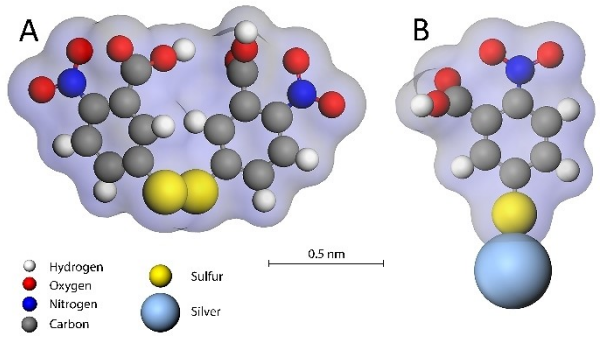

Figure 5. Models of (A) DTNB molecule and (B) TNB molecule on the silver atom.

energy. Breaking up of DTNB disulfide bonds resulted in adsorption of the TNB products on the substrate enriched with the surface states. The adsorbed molecules had to be strongly anchored on the surface. At the same time, if the TNB molecules were densely packed (*i.e.* were in excess) they could be reverted in the DTNB state in a course of ethanol evaporation (while samples' drying). These DTNB molecules coalesced and formed nanoclusters. That is why the SERS-spectra of the samples with relatively high concentration were found to contain the 510 cm^{-1} band associated with the disulfide bond.

Finally, we studied how the SERS maps were changing while the molecules' concentration was getting closer to the single molecule level. Pursuing this goal we performed the SERS scanning of the dendritic substrates kept in the 10^{-12}–10^{-18} M solutions of DTNB using the ×100 objective with NA = 1.4. It provided a small laser spot of ~0.55 μm diameter. The recorded SERS spectra arrays were processed and represented as SERS maps reflecting distribution of the analyte molecules over the substrate (Figure 6). The SERS map of the 10^{-12} M sample was characterized by the SERS-spectra with the S–S band and free of it (Figure 6A). This means that the sample had the DTNB nanoclusters but their density was not enough for prevalence of disulfide-containing signatures in all the spectra. This argument was in good agreement with the SEM data. During scanning the 10^{-12} M sample, the laser could overlap two types of areas: (i) DTNB nanocluster, which corresponds to the red point on the SERS map in Figure 6A, and (ii) TNB layer without DTNB nanocluster (other not black points on the SERS map in Figure 6A). Assuming volume of the observed nanocluster (90 nm^3) and of the DTNB molecule (0.34 nm^3), the single nanocluster contained approximately 264 DTNB molecules, *i.e.* this number of molecules was detected in the red point. The SERS-intensity in the points around DTNB nanocluster was higher than that in distance from it. This could be caused by denser monomolecular TNB layer, which localized near the nanocluster while its formation.

The SERS-maps of the 10^{-14}–10^{-18} M samples were constituted by only TNB residues spectra, as no S–S-related bands were observed in them (Figure 6B–D). This led to conclusion that the SERS-signals were induced by only monomolecular TNB layer. To reveal the minimal number of the TNB molecules that could be detected with the dendritic SERS-active substrate we first studied the map recorded on the sample with the attomolar concentration of analyte.

Assuming that all the molecules were adsorbed on the 4 mm^2 substrate from the 1 ml solution it was calculated that six 24×24 μm^2 maps contained one TNB product (one DTNB molecule provided two TNB molecules). This was in a good agreement with the repeatability of the informative signal detection while SERS-measurements. Therefore, the only one informative SERS-spectrum recorded on the map in Figure 6D was a signature of the single TNB molecule. An intensity of its signal was nearly twice lower than that of the less intensive SERS-spectra marked as dark blue squares on map corresponded to the 10^{-16} M concentration, *i.e.* each of these points contained two TNB molecules. The same prediction way of a number of imaged TNB molecules could be applied for other SERS maps.

3. Conclusion

3D silver nanostructures, which consisted of Ag NPs and network of volumetric densely-packed Ag dendrites deposited on the surface of macro-PS, were fabricated and comprehensively investigated. Silver deposition was carried out by the wet chemical corrosion method from the solution containing $AgNO_3$ salt, ethanol and small amount of hydrofluoric acid. Before the deposition of Ag, the macro-PS surface was subjected to the treatment with argon plasma to give it a slight roughness that provided improved adhesion of the dendritic layer to the template. It was found, that Ag precipitates selectively deposited on the outer rough surface of the macro-PS skeleton and were completely absent in the pore channels. This effect was explained by the catalytic action of Ag NPs formed almost immediately after the macro-PS skeleton surface contacted with the solution. On such a surface, Ag NPs, vertical and lateral dendrites were deposited after initial nucleation on the sharp parts of the roughened surface of the macro-PS skeleton.

Optical reflectance spectroscopy of the silver dendrites revealed the three light absorption bands related to the combination of different SPR modes. Their positions were found to coincide with blue, red and near infrared wavelengths. Computer simulations of electric field distribution in the silver dendrites on macro-PS showed that they are prospective to be SERS-active upon the excitation with 473, 633 and 785 nm lasers that are widely used in vibrational spectroscopy and other techniques of optical analysis. For the first time, we experimentally demonstrated that the analyte molecules tend to coalescence into the DTNB nanoclusters rather than to form the single-molecule layer of TNB on the surface of the SERS-active substrates at concentrations over 10^{-12} M. The DTNB nanoclusters were formed from the 10^{-6}–10^{-12} M solutions, while further decrease in the analyte molecules down to the attomolar concentration was favorable for the adsorption of the TNB molecules' single layer. SERS imaging of the single TNB molecule was demonstrated with the SERS-active silver dendrites kept in the attomolar DTNB solution.

© 2020 Wiley-VCH GmbH

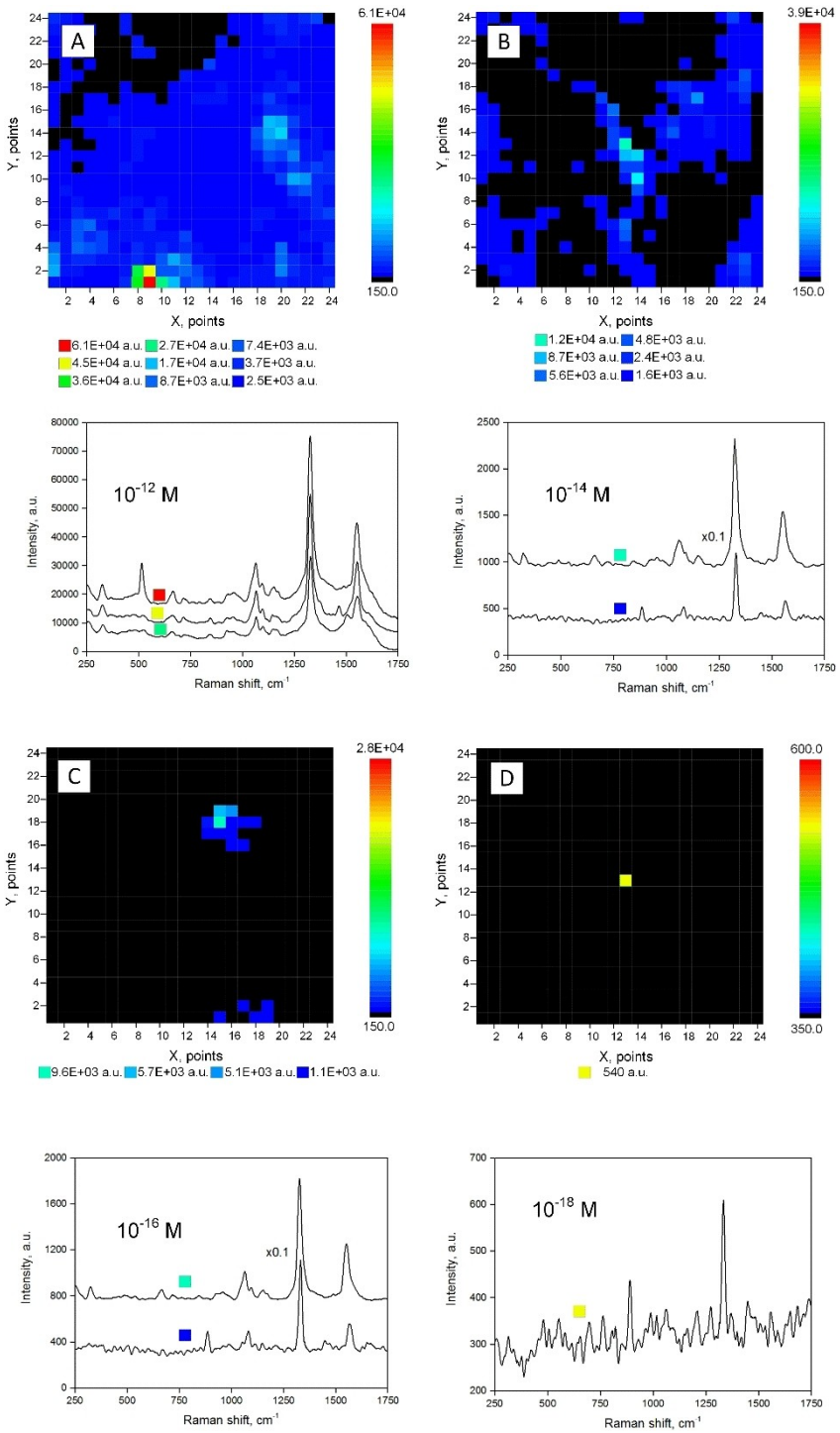

Figure 6. SERS-imaging of the (A) DTNB/TNB and (B–D) TNB adsorbed on the silver dendrites on macro-PS from DTNB solutions of (A) 10^{-12} M, (B) 10^{-14} M, (C) 10^{-16} M and (D) 10^{-18} M concentrations. SERS-intensity was measured in 1335 cm^{-1} band. SERS-spectra were smoothed using Savitzky-Golay filter (10 window points, 2nd polynomial order).

Experimental Section/Methods

Materials: Silver nitride (≥99.0%), ethanol (≥99.5%), hydrofluoric acid (48 wt.% in H_2O), dimethyl sulfoxide (≥99.9%), and DTNB (99.0%) were purchased from Sigma-Aldrich and used without additional purification. Boron-doped (100) silicon wafers (University Wafer, Boston, MA, USA) were double-side polished and had 100 mm diameter, 525±15 μm thickness and resistivity of 1–10 Ohm cm. Water was purified with Milli-Q system (Millipore, Bedford, MA, USA).

Fabrication of macroporous silicon template: Si wafers with parameters described in the previous subsection were used as initial substrates. Chemical cleaning and removal of a native oxide were

© 2020 Wiley-VCH GmbH

performed by standard techniques based on Radio Corporation of America (RCA) chemical solutions[54] and 5% water solution of hydrofluoric acid, respectively. The wafers were cut into 2.5× 2.5 cm^2 square samples. The macro-PS layers with pore diameters of 1.2–1.5 μm and thickness of 5 μm were formed by an electrochemical anodization in a mixture of hydrofluoric acid and dimethyl sulfoxide according to the slightly modified procedure reported elsewhere.[55] No illumination of the sample surface was used. The anodization process was carried out in a galvanostatic mode at a current density of 8 mA cm^{-2} over 10 min. A Metrohm AUTOLAB PGSTAT 302 N potentiostat/galvanostat (Metrohm Autolab, Utrecht, The Netherlands) was used for anodization.

Silver deposition: To provide the selective deposition of Ag on the Si skeleton tops we subjected the external surface of the macro-PS to a slight roughening by ion-beam plasma etching in ORTUS camera (IZOVAK, Minsk, Belarus) at a voltage of 2.5 kV and a discharge current of 60 mA in argon plasma. Immediately after that, the macro-PS samples were immersed in a solution of 12 mM $AgNO_3$, 1 M C_2H_5OH and 3 M HF. The Ag deposition process lasted for 3 min at room temperature. The final substrates were cut to have a SERS-active area of 4 mm^2 (rectangular 2×2 mm^2 samples).

Structural and optical characterization: Reflectance spectra of the samples were recorded using an MC122 spectrophotometer (Proscan Special Instruments, Minsk, Belarus) in a 350–800 nm range. The structure of the samples was studied by SEM (Hitachi S-4800; Hitachi, Tokyo, Japan) and AFM (NTEGRA Prima; NT-MTD, Zelenograd, Russia) in semi-contact scanning mode. The ImageJ2x software was used to make a statistical analysis of the SEM and AFM images to evaluate a number of the Ag NPs and Ag dendrites formed on the surface of the macro-PS samples, mean sizes of the Ag nanostructures, and coverage of the samples' surface with them.

Computer simulations: Simulation of an electric field in the silver dendrites of chevron-like morphology on the macro-PS samples were performed using COMSOL AC/DC Module as described elsewhere.[56] In more detail we solved a 3D frequency-domain wave equation for the electric field with a finite element method in order to obtain the electric field distribution. To simulate the excitation laser light we used a plane wave with a normal incidence in the full-field formulation. The wave propagated in a negative y-direction. The incident power density was 10^5 W·cm^{-2}. Materials Studio BIOVIA software was used for structure visualization of target molecules and volume calculation.

SERS-measurements: For the SERS-measurements, the dendritic substrates were immersed into 1 ml of ethanol solutions containing DTNB for 1 h and then rinsed to remove an excess of non-adsorbed molecules. We first prepared the basic solutions of the analytes with a 10^{-2} M concentration that was further gradually decreased by successive dilution with the solvent. In this work, the SERS-measurements were carried out for the analyte at the 10^{-6}–10^{-18} M concentrations. We exploited "Confotec CARS" microspectrometer (SOL Instruments Ltd., Minsk, Belarus). This is a scanning laser microspectrometer coupled to the NIKON TE2000-E inverted microscope (Nikon Corp., Tokyo, Japan) and comprises a picosecond laser source for CARS option and 633 nm He–Ne laser (model 05-LHP-991, Melles Griot, Albuquerque, New Mexico) for the Raman and SERS measurements. The laser power at the sample was controlled by a variable neutral filter with the 0–3 optical density. The samples at "Confotec CARS" were located at the motorized sample position adjustment stage (model H117TE, Prior Scientific Instruments, Cambridge, UK). A Peltier-cooled CCD camera ProScan HS-101H (Proscan Electronic Systems, Scheuring, Germany) was used for detection of the spectra collected in the backscattering geometry. We probed signals in the 250–1750 cm^{-1} range of vibrational frequencies with the resolution of 1.8 cm^{-1}. Rayleigh scattering was blocked using Semrock long-pass edge filters. During the SERS-measurements 24×24 $μm^2$ surface areas of the substrate were scanned with a step of 1 μm. The SERS scanning was performed in two stages pursuing goals to (i) define detection limit and (ii) realize single-molecule imaging as described in Results and Discussion section. Objective used to focus the laser on the substrate provided ×40 (LUCPLFN; NA = 0.6, air/dry) and ×100 (HC PLAPO CS2; NA = 1.4, oil) magnifications with ~1.3 μm and ~0.55 μm light spots, respectively. The laser power density was adjusted to $(1 \pm 0.2)\cdot 10^5$ W/cm^{-2} after passing through optical system and objective. The exposure time was 1 s for each point of the SERS-map. All measurements were performed at room temperature.

Acknowledgements

The authors would like to gratefully acknowledge Prof. Vitaly P. Bondarenko from Belarusian State University of Informatics and Radioelectronics for fruitful discussions on porous silicon properties and Prof. Bruno Azeredo from Arizona State University for his valuable suggestions and comments on the manuscript preparation. The present research has been financially supported in parts by the U.S. Department of State (Fulbright Grant, # PS00284506), the Ministry of Education of the Republic of Belarus (Belarusian National Research Program "Photonics, opto- and microelectronics", tasks 1.4.01 and 3.3.07), State Committee on Science and Technology of the Republic of Belarus (F19UKRG-006) and Topical Plan for JINR Research and International Cooperation (theme # 04-4-1133).

Conflict of Interest

The authors declare no conflict of interest.

Keywords: single-molecule imaging · attomolar concentration, surface-enhanced Raman scattering · silver dendrites · DTNB · disulfide bonds

[1] S. Gaponenko, H. V. Demir, C. Seassal, U. Woggon, *Opt. Express* **2016**, *24*, A430.
[2] D. G. Baranov, A. Krasnok, T. Shegai, A. Alù, Y. Chong, *Nat. Rev. Mater.* **2017**, *2*, 17064.
[3] C. Ng, L. Wesemann, E. Panchenko, J. Song, T. J. Davis, A. Roberts, D. E. Gómez, *Adv. Opt. Mater.* **2019**, *7*, 1801660.
[4] L. He, E. Lamont, B. Veeregowda, S. Sreevatsan, C. L. Haynes, F. Diez-Gonzalez, T. P. Labuza, *Chem. Sci.* **2011**, *2*, 1579.
[5] J. E. L. Villa, M. A. S. Afonso, D. P. dos Santos, P. A. Mercadal, E. A. Coronado, R. J. Poppi, *Spectrochim. Acta Part A* **2020**, *224*, 117380.
[6] E. C. Le Ru, M. Meyer, P. G. Etchegoin, *J. Phys. Chem. B* **2006**, *110*, 1944.
[7] M. Kerker, *Acc. Chem. Res.* **1984**, *17*, 271.
[8] K. Kneipp, Y. Wang, H. Kneipp, L. T. Perelman, I. Itzkan, R. R. Dasari, M. S. Feld, *Phys. Rev. Lett.* **1997**, *78*, 1667.
[9] L. Litti, A. Ramundo, F. Biscaglia, G. Toffoli, M. Gobbo, M. Meneghetti, *J. Colloid Interface Sci.* **2019**, *533*, 621.
[10] E. P. Hoppmann, W. W. Yu, I. M. White, *Methods* **2013**, *63*, 219.
[11] A. Pimentel, A. Araújo, B. Coelho, D. Nunes, M. Oliveira, M. Mendes, H. Águas, R. Martins, E. Fortunato, *Materials* **2017**, *10*, 1351.
[12] J. A. Lartey, J. P. Harms, R. Frimpong, C. C. Mulligan, J. D. Driskell, J.-H. Kim, *RSC Adv.* **2019**, *9*, 32535.
[13] S. D. Bindesri, D. S. Alhatab, C. L. Brosseau, *Analyst* **2018**, *143*, 4128.

© 2020 Wiley-VCH GmbH

[14] S. Fateixa, P. C. Pinheiro, H. I. S. Nogueira, T. Trindade, *J. Mol. Struct.* **2019**, *1185*, 333.
[15] A. Lamberti, A. Virga, A. Angelini, A. Ricci, E. Descrovi, M. Cocuzza, F. Giorgis, *RSC Adv.* **2015**, *5*, 4404.
[16] Y. Kalachyova, M. Erzina, P. Postnikov, V. Svorcik, O. Lyutakov, *Appl. Surf. Sci.* **2018**, *458*, 95.
[17] L. Zeiri, *J. Raman Spectrosc.* **2007**, *38*, 950.
[18] N. Ferreira, A. Marques, H. Águas, H. Bandarenka, R. Martins, C. Bodo, B. Costa-Silva, E. Fortunato, *ACS Sens.* **2019**, *4*, 2073.
[19] R. J. Walsh, G. Chumanov, *Appl. Spectrosc.* **2001**, *55*, 1695.
[20] H. K. Park, J. K. Yoon, K. Kim, *Langmuir* **2006**, *22*, 1626.
[21] E. Babich, A. Redkov, I. Reduto, A. Lipovskii, *Phys. Status Solidi RRL* **2018**, *12*, 1700226.
[22] A. Kaminska, O. Inya-Agha, R. J. Forster, T. E. Keyes, *Phys. Chem. Chem. Phys.* **2008**, *10*, 4172.
[23] T. Wang, Z. Zhang, F. Liao, Q. Cai, Y. Li, S.-T. Lee, M. Shao, *Sci. Rep.* **2015**, *4*, 4052.
[24] M. E. Koleva, N. N. Nedyalkov, R. Nikov, R. Nikov, G. Atanasova, D. Karashanova, V. I. Nuzhdin, V. F. Valeev, A. M. Rogov, A. L. Stepanov, *Appl. Surf. Sci.* **2020**, *508*, 145227.
[25] K. Kneipp, A. S. Haka, H. Kneipp, K. Badizadegan, N. Yoshizawa, C. Boone, K. E. Shafer-Peltier, J. T. Motz, R. R. Dasari, M. S. Feld, *Appl. Spectrosc.* **2002**, *56*, 150.
[26] P. Etchegoin, R. Maher, L. Cohen, H. Hartigan, R. J. Brown, M. J. Milton, J. Gallop, *Chem. Phys. Lett.* **2003**, *375*, 84.
[27] A. J. Wright, J. L. Richens, J. P. Bramble, N. Cathcart, V. Kitaev, P. O'Shea, A. J. Hudson, *Nanoscale* **2016**, *8*, 16395.
[28] R. Tantra, R. J. C. Brown, M. J. T. Milton, *J. Raman Spectrosc.* **2007**, *38*, 1469.
[29] A. Campion, J. E. Ivanecky, C. M. Child, M. Foster, *J. Am. Chem. Soc.* **1995**, *117*, 11807.
[30] G. C. Schatz, M. A. Young, R. P. Duyne, in *Surface-Enhanced Raman Scattering*, Springer Berlin Heidelberg, **2006**, pp. 19–45.
[31] E. C. Le Ru, E. Blackie, M. Meyer, P. G. Etchegoin, *J. Phys. Chem. C* **2007**, *111*, 13794.
[32] Pilot, Signorini, Durante, Orian, Bhamidipati, Fabris, *Biosensors* **2019**, *9*, 57.
[33] P. Mosier-Boss, *Nanomaterials* **2017**, *7*, 142.
[34] T. Bora, in *Noble and Precious Metals - Properties, Nanoscale Effects and Applications*, InTech, **2018**.
[35] C. Y. Zhang, Y. Lu, B. Zhao, Y. W. Hao, Y. Q. Liu, *Appl. Surf. Sci.* **2016**, *377*, 167–173.
[36] M. J. Lo Faro, C. D'Andrea, A. A. Leonardi, D. Morganti, A. Irrera, B. Fazio, *Nanomaterials* **2019**, *9*, 1630.
[37] X.-L. Tang, P. Jiang, G.-L. Ge, M. Tsuji, S.-S. Xie, Y.-J. Guo, *Langmuir* **2008**, *24*, 1763.
[38] L. Wang, H. Li, J. Tian, X. Sun, *ACS Appl. Mater. Interfaces* **2010**, *2*, 2987.
[39] H. S. S. Sharma, E. Carmichael, D. McCall, *Vib. Spectrosc.* **2016**, *83*, 159.
[40] C. Yang, Y. Xu, M. Wang, T. Li, Y. Huo, C. Yang, B. Man, *Opt. Express* **2018**, *26*, 10023.
[41] E. J. Titus, M. L. Weber, S. M. Stranahan, K. A. Willets, *Nano Lett.* **2012**, *12*, 5103.
[42] M. Ishikawa, Y. Maruyama, J. Y. Ye, M. Futamata, *J. Biol. Phys.* **2002**, *28*, 573.
[43] N. C. Lindquist, C. D. L. de Albuquerque, R. G. Sobral-Filho, I. Paci, A. G. Brolo, *Nat. Nanotechnol.* **2019**, *14*, 981.
[44] G. Arzumanyan, N. Doroshkevich, K. Mamatkulov, S. Shashkov, K. Girel, H. Bandarenka, V. Borisenko, *Phys. Status Solidi*, **2017**, *214*, 1600915.
[45] Q. Ma, Y.-L. Li, N.-C. Gong, X. Jiang, S.-Y. Huan, *Chin. J. Anal. Chem.* **2015**, *43*, 1676.
[46] N. N. Yazgan, İ. H. Boyacı, E. Temur, U. Tamer, A. Topcu, *Talanta* **2010**, *82*, 631.
[47] D. Yakimchuk, E. Kaniukov, V. Bundyukova, L. Osminkina, S. Teichert, S. Demyanov, V. Sivakov, *MRS Commun.* **2018**, *8*, 95.
[48] W. Ye, C. Shen, J. Tian, C. Wang, L. Bao, H. Gao, *Electrochem. Commun.* **2008**, *10*, 625.
[49] M. K. Oh, H. J. Baik, S. K. Kim, S. Park, *J. Mater. Chem.* **2011**, *21*, 19069.
[50] A. G. Cullis, L. T. Canham, P. D. J. Calcott, *J. Appl. Phys.* **1997**, *82*, 909.
[51] Y. K. Shrestha, F. Yan, *RSC Adv.* **2014**, *4*, 37274.
[52] D. Kurouski, J. Washington, M. Ozbil, R. Prabhakar, A. Shekhtman, I. K. Lednev, *PLoS One* **2012**, *7*, e36989.
[53] R. G. Nuzzo, D. L. Allara, *J. Am. Chem. Soc.* **1983**, *105*, 4481.
[54] A. Dolgiy, S. V. Redko, H. Bandarenka, S. L. Prischepa, K. Yanushkevich, P. Nenzi, M. Balucani, V. Bondarenko, *J. Electrochem. Soc.* **2012**, *159*, D623.
[55] I. Khodasevich, A. Panarin, S. Terekhov, K. Artsemyeva, A. Dolgiy, H. Bandarenka, V. Bondarenko, *ECS Trans.* **2013**, *53*, 85.
[56] S. Redko, A. Dolgiy, D. Zhygulin, V. Khaliava, N. Khinevich, S. Zavatski, H. Bandarenka, *SPIE* **2019**, *10912*, 109121O.

Manuscript received: September 23, 2020
Revised manuscript received: November 2, 2020
Accepted manuscript online: November 4, 2020
Version of record online: ■■, ■■■

© 2020 Wiley-VCH GmbH

FULL PAPER

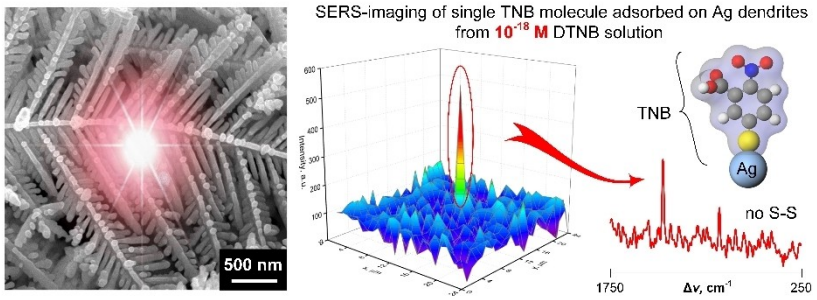

Reliable imaging of single molecules by surface-enhanced Raman spectroscopy (SERS) is a challenge while using solid SERS-active substrates. In present work tightly-packed 3D silver dendrites are developed to achieve SERS-imaging of individual DTNB (5,5′-dithio-bis-[2-nitrobenzoic acid]) nanoclusters and TNB molecules adsorbed on the silver surface from 10^{-6}–10^{-18} M solutions of DTNB, which is an essential molecule for chemical/biomedical analysis.

Prof. H. V. Bandarenka, N. V. Khinevich, A. A. Burko, S. V. Redko, S. A. Zavatski, U. A. Shapel, Dr. K. Z. Mamatkulov, M. Y. Vorobyeva, Prof. G. M. Arzumanyan**